Comparison of Quantization Schemes

We now apply the results of the analysis of R_0' to the evaluation of certain interesting quantization schemes. As usual, we assume that the transmission is corrupted by additive white Gaussian noise.

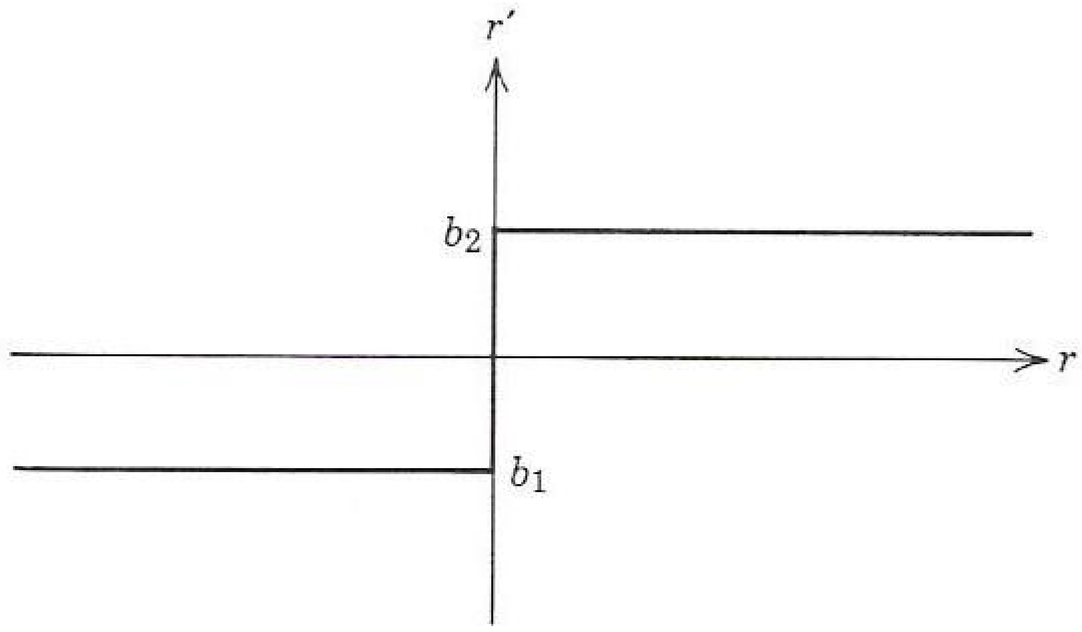

Figure 6.19 Quantizer for binary symmetric channel; $A = 2$, $Q = 2$.

Binary input, binary output. In the first case that we consider the transmitter alphabet consists of only two allowable input amplitudes,

$$a_1 = +\sqrt{E_N}$$
$$a_2 = -\sqrt{E_N}. \tag{6.68}$$

The matched filter output at the receiver is also quantized into two levels, as shown in Fig. 6.19. Thus $A = 2$, $Q = 2$, and the overall channel diagram is that of Fig. 6.20, in which

$$q_{12} = q_{21} \triangleq p \tag{6.69a}$$

$$q_{11} = q_{22} = 1 - p \tag{6.69b}$$

and

$$p = Q(\sqrt{2E_N/\mathcal{N}_0}). \tag{6.69c}$$

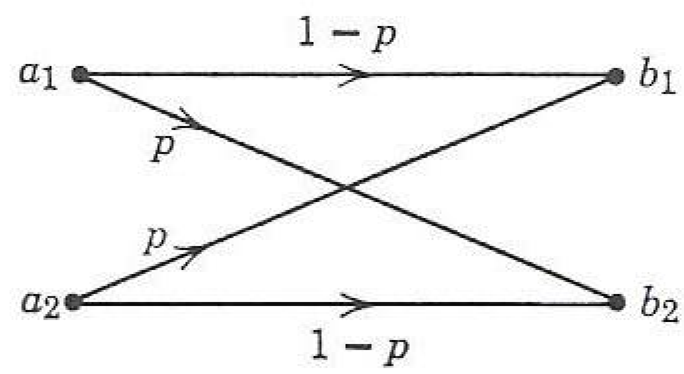

Figure 6.20 Transition diagram for binary symmetric channel.

The transition diagram is that of a *binary symmetric channel* (BSC). Because of the symmetry of this channel, the probability assignment $p_1 = p_2 = \frac{1}{2}$ is optimum. From Eq. 6.62b we then have

$$\begin{aligned} R_0' &= -\log_2 \sum_{h=1}^{2} \left[\sum_{l=1}^{2} p_l \sqrt{q_{lh}} \right]^2 \\ &= -\log_2 [(\tfrac{1}{2}\sqrt{p} + \tfrac{1}{2}\sqrt{1-p})^2 + (\tfrac{1}{2}\sqrt{p} + \tfrac{1}{2}\sqrt{1-p})^2] \\ &= 1 - \log_2 [1 + 2\sqrt{p(1-p)}]. \end{aligned} \tag{6.70}$$

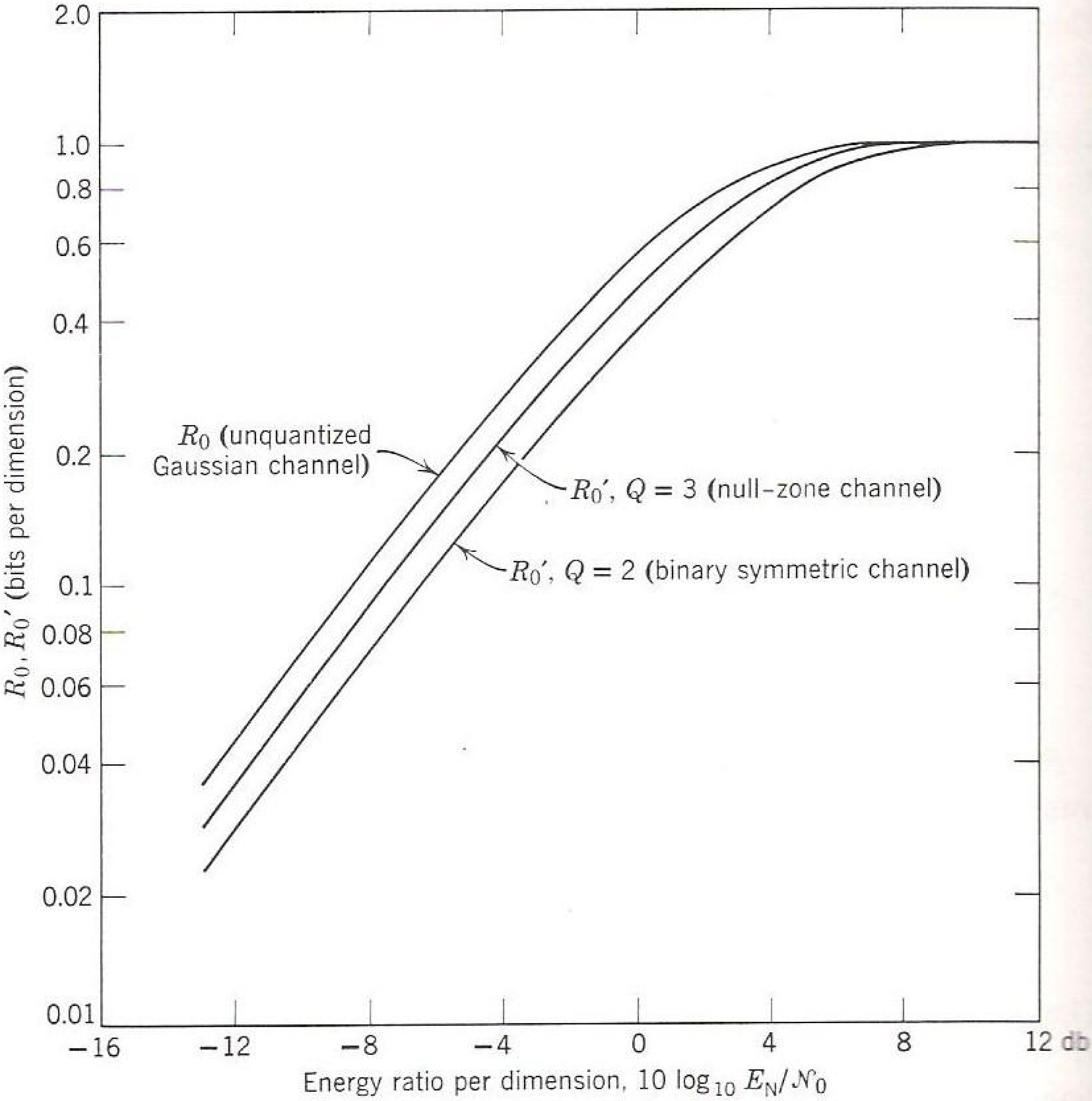

Figure 6.21 R_0 and R_0' for binary antipodal signaling with two- and three-level symmetric quantization.

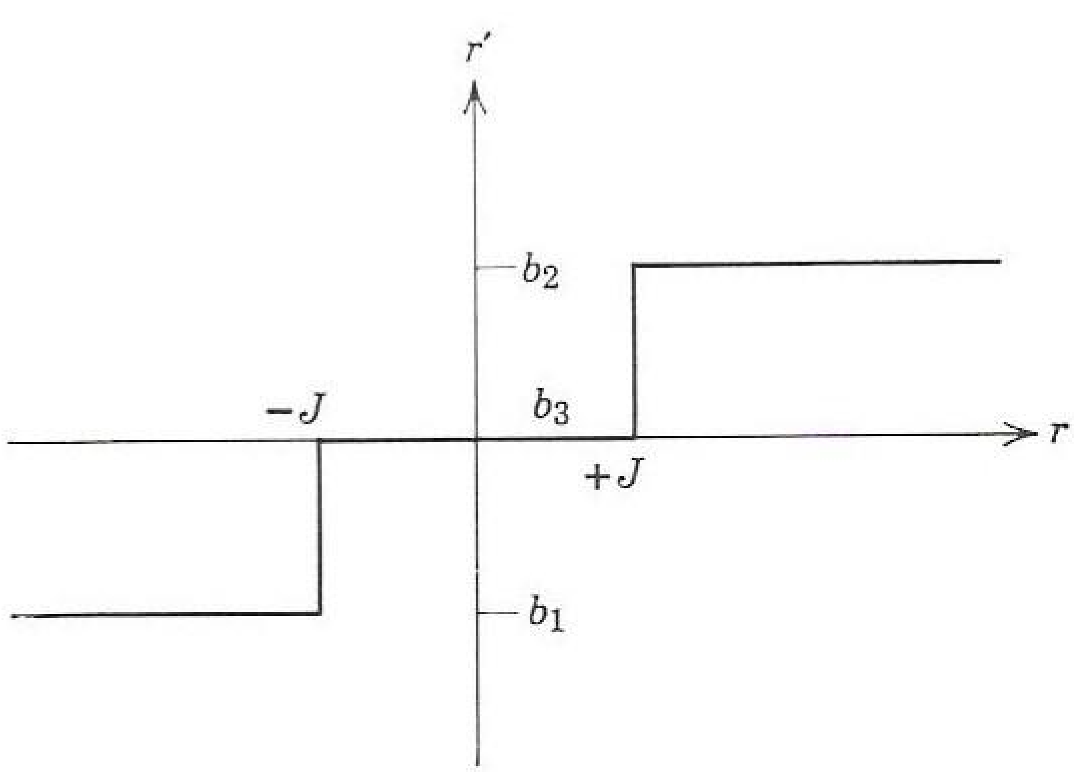

Figure 6.22 Quantizer for null-zone channel, $A = 2$, $Q = 3$.

The value of R_0' from Eq. 6.70 is plotted in Fig. 6.21 as a function of $E_N/\mathcal{N}_0$, together with the unquantized R_0 given by Eq. 6.67. We observe that the quantization loss is approximately -2 db. More precisely, in the limit $E_N/\mathcal{N}_0 \to 0$ (hence $p \to \frac{1}{2}$) it can be shown that the loss in decibels is exactly $10 \log_{10} (2/\pi)$.

Binary input, ternary output. A significant fraction of the degradation in R_0' resulting from binary quantization can be avoided by going to a ternary output. For $A = 2$, $Q = 3$ the appropriate quantizer is that shown in Fig. 6.22 and the resulting over-all channel diagram is that of Fig. 6.23. We have

$$q_{12} = q_{21} \triangleq p \qquad (6.71a)$$

$$q_{13} = q_{23} \triangleq w \qquad (6.71b)$$

and

$$q_{11} = q_{22} = 1 - p - w, \qquad (6.71c)$$

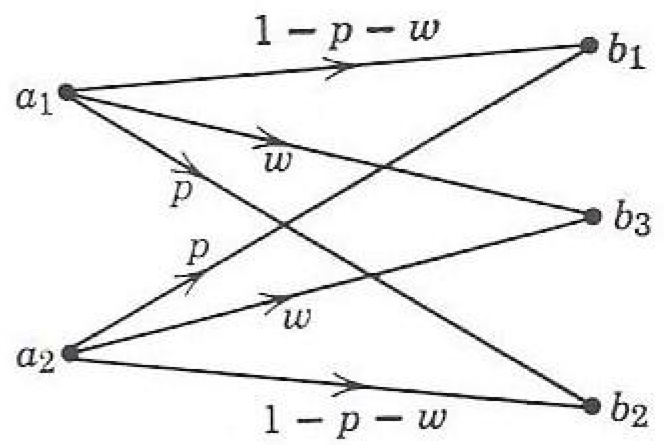

Figure 6.23 Transition probability diagram for null-zone channel.

where p and w are given in terms of the quantizer threshold J by the equations

$$p = \int_J^\infty \frac{1}{\sqrt{\pi \mathcal{N}_0}} e^{-(y+\sqrt{E_N})^2/\mathcal{N}_0}\, dy \qquad (6.72a)$$

$$w = \int_{-J}^{J} \frac{1}{\sqrt{\pi \mathcal{N}_0}} e^{-(y+\sqrt{E_N})^2/\mathcal{N}_0}\, dy. \qquad (6.72b)$$

Such a channel is called either a *null-zone channel* or a *binary symmetric erasure channel* (abbreviated BSEC). By symmetry we again choose $p_1 = p_2 = \frac{1}{2}$. Then, from Eq. 6.62b, we have

$$\begin{aligned} R_0' &= -\log_2 \sum_{h=1}^{3} \left[\sum_{l=1}^{2} p_l \sqrt{q_{lh}} \right]^2 \\ &= -\log_2 [(\tfrac{1}{2}\sqrt{1-p-w} + \tfrac{1}{2}\sqrt{p})^2 + (\tfrac{1}{2}\sqrt{w} + \tfrac{1}{2}\sqrt{w})^2 \\ &\quad + (\tfrac{1}{2}\sqrt{1-p-w} + \tfrac{1}{2}\sqrt{p})]^2 \\ &= 1 - \log_2 [1 + w + 2\sqrt{p(1-p-w)}]. \end{aligned} \qquad (6.73)$$

The value of R_0' given by Eq. 6.73 is a function of the quantizer threshold value, J. The optimum value of J (the value that maximizes R_0') can be found as a function of $E_N/\mathcal{N}_0$ by trial and error; it is plotted in Fig. 6.24. The value of R_0' resulting from Eq. 6.73 when J is optimum is plotted as a function of $E_N/\mathcal{N}_0$ in Fig. 6.21. We observe that the degradation from the unquantized case is roughly 1 db and conclude that

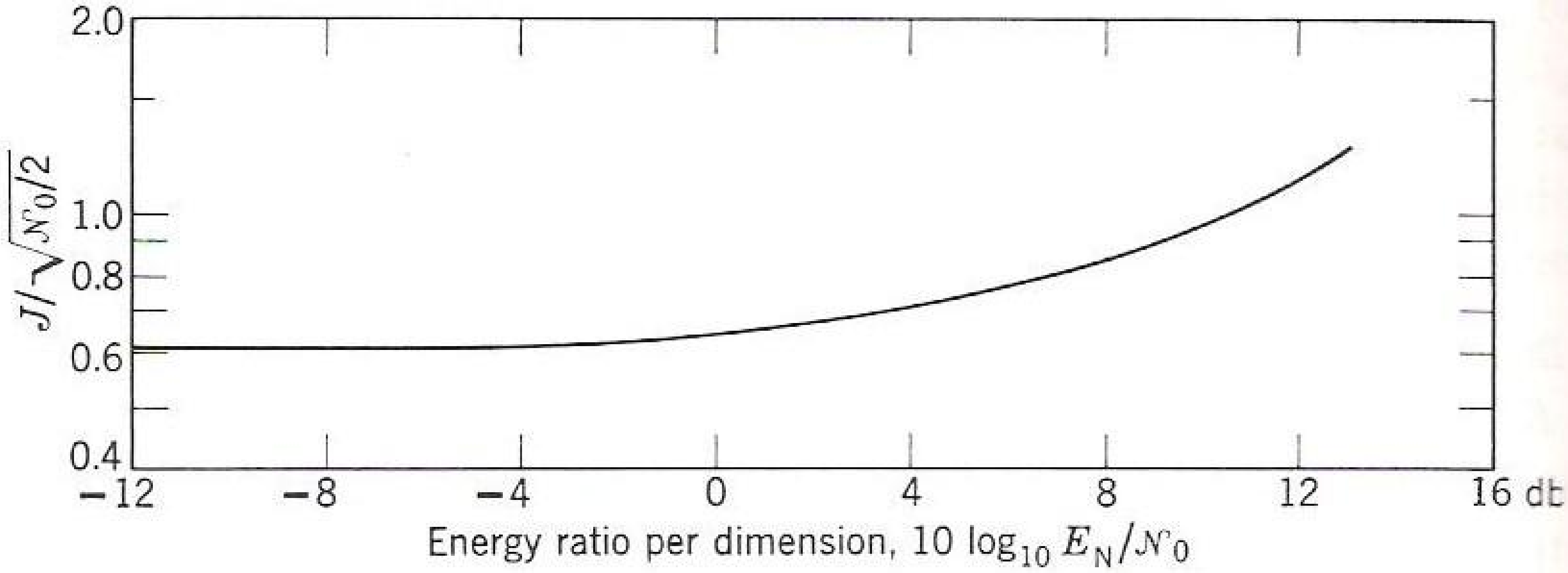

Figure 6.24 Optimum threshold for null-zone channel.

little improvement can be gained by quantizing to more than three levels when $E_N/\mathcal{N}_0$ is sufficiently small that signaling with sequences of binary waveforms is efficient. Note in Fig. 6.24 that $J = 0.65\sqrt{\mathcal{N}_0/2}$ is near optimum over this interesting range of $E_N/\mathcal{N}_0$.

Multiamplitude inputs. Quantization at the receiver also implies a degraded R_0' for systems that employ a multiamplitude modulator to exploit a high energy-to-noise ratio per dimension. For a given input alphabet $\{a_l\}$ and a given quantization grid the first step in evaluating the degradation is to determine the transition probabilities $\{q_{lh}\}$ in accordance with Fig. 6.16. The second step is to substitute these $\{q_{lh}\}$, together with an appropriate choice of letter probabilities $\{p_l\}$, into the expression

$$R_0' = -\log_2 \sum_{h=1}^{Q} \left[\sum_{l=1}^{A} p_l \sqrt{q_{lh}} \right]^2. \tag{6.74}$$

We now apply these results to a particular ensemble of systems operating over an additive white Gaussian noise channel. Each system utilizes a modulator with transmitter letters $\{a_l\}$ equally spaced over the interval $[-\sqrt{E_N}, +\sqrt{E_N}]$ and a receiver with a uniform quantization grid similar to that shown in Fig. 6.25 for $A = 6$; the number, Q, of quantizer output levels is equal to the number, A, of transmitter letters.

Curves of R_0' as a function of $E_N/\mathcal{N}_0$ for $Q = A = 2, 3, 4, 8, 16, 32$, and 64, calculated on a computer, are plotted in Fig. 6.26. In each case the letter probabilities $\{p_l\}$ have been set equal to $1/A$. For reference, the

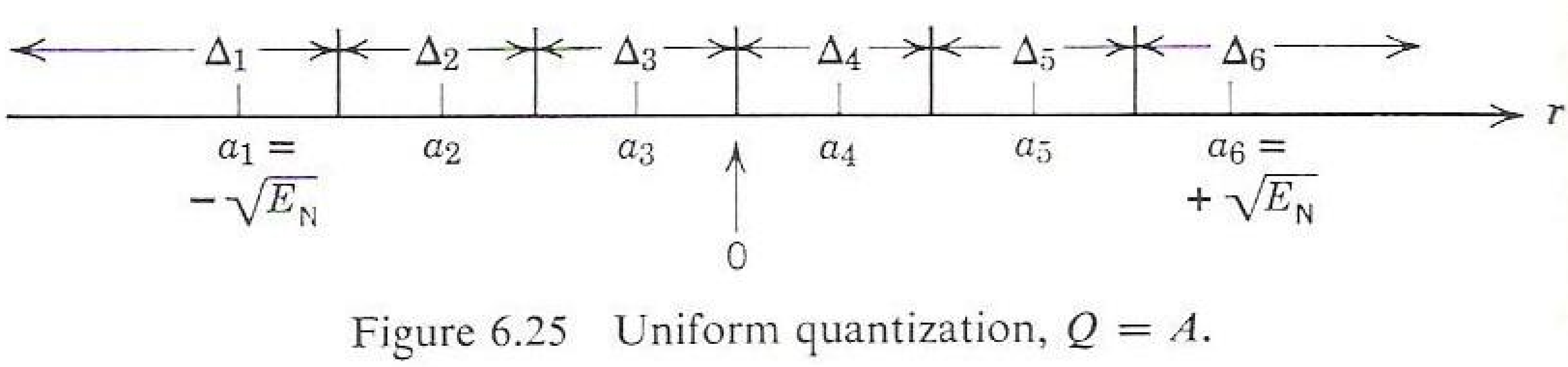

Figure 6.25 Uniform quantization, $Q = A$.